DETERMINATION OF INTERFACIAL PROPERTIES

FINAL REPORT FOR THE PERIOD
February 20, 1989 through August 19, 1991

CONTRACT NO. N00014-89-C-0083

Prepared for:

Dr. Thomas M. Donnellan
Naval Air Development Center
Code 6064
Warminster, PA 18974

Submitted by

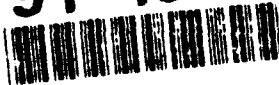Dr. Michael R. James
Dr. Winfred L. Morris
Dr. Mahyar S. Dadkhah

NOVEMBER 1991

Rockwell International
Science Center

The Contractor, Rockwell International Corporation Science Center, hereby certifies that, to the best of its knowledge and belief, the technical data delivered herewith under Contract No. N00014-89-C-0083 is complete, accurate, and complies with all requirements of the contract.

12 Dec 91
Date

M.R. Stan
Name and Title of Certifying Official

TABLE OF CONTENTS

FIGURE CAPTIONS

FIGURE CAPTIONS

Statement A per telecon Dr. A K Vasudevan
ONR/Code 1222
Arlington, VA 22217-5000

NWW 1/8/92

1.0   INTRODUCTION

The primary objective of this program was to determine surface displacements in the resin matrix adjacent to a graphite fiber during applied fiber strain. These data are to be used in the NADC Interfaces in Organic Matrix Composites Program to quantify the effect of interphases on fiber-matrix interfacial elastic properties. We successfully demonstrated the measurement of in- and out-of-plane displacement fields with sufficient spatial resolution to produce data for calculating the modulus and thickness of interphase layers in the epoxy within a few microns of the graphite fiber. The interphase layer was modified by using different surface treatments and coatings applied to the AS-4 fibers.

The shear lag and finite element models used by NADC and ourselves to model the interphase are elastic. Our initial efforts at measuring surface displacement indicated that significant inelastic effects occurred during first load. At fiber strains above 0.4%, the inelastic effect could be shaken-out or relaxed by cyclic loading, after which the measured displacements were elastic and showed significant influence of the fiber surface treatment. However, substantial changes in the matrix could have occurred during the relaxatic.1 process, including microcracking of the interface. To minimize such potential damage, a new measurement technique was developed to determine surface displacements at low loads where the interphase properties were elastic. Measurement of the small displacements induced by the low fiber strains of less than 0.1% required the improved sensitivity obtained by a unique approach to recording SEM images of surface displacements resulting from load changes during image recording.

Except for the phenolic coated specimens, all surface treatments/coatings show an apparent decrease in the interphase modulus as the maximum strain applied to the fiber is raised. It is now clear that this is largely due to damage to the material near the fiber/matrix interface. For the uncoated fibers, the maximum strain need not be much larger than 0.1% for the interphase to be damaged. The interphase of sized fiber specimens loaded below 0.1% fiber strain were clearly elastic as were the phenolic coated specimens at loads up to 0.4% fiber strain. Because of the higher relative noise levels at the small displacements (low loads), it was difficult to detect small differences in interphase deformation. Careful statistical assessment of models fit to the data by NADC will be needed to determine quantitative influences of different coatings on the interphase properties.

2.0 HIGH SPATIAL RESOLUTION DISPLACEMENT MEASUREMENT TECHNIQUES

Stereoimaging displacement analysis was used to obtain the necessary sub-micron spatial resolution and high displacement sensitivity required in this program. With this technique, one measures differential displacements from pairs of SEM or optical micrographs consisting of one taken before and one taken after the application of a mechanical or thermal load. If the micrographs are recorded with the sample normal to the viewing axis (Fig. 1), in-plane displacements are found. If the sample is tilted, a combination of in- and out-of-plane displacements are sensed, from which the out-of-plane displacement can be calculated (1,2). The measured displacements are differential, that is, they represent change due to application of a load. They are also made relative to one point or feature on the micrograph. In the present case this means that the displacement of the matrix is made relative to the fiber. Topographical measurements of just surface height can be obtained in a similar way using micrographs recorded at two different tilt angles, as in traditional stereo-microscopy, but such data do not have the desired accuracy.
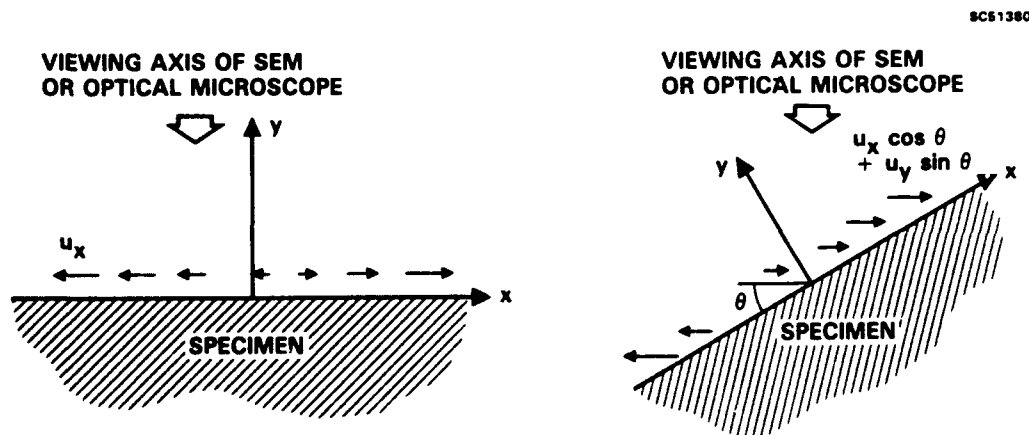
Fig. 1   (a) With normal viewing only in-plane displacements are sensed;   (b) by tilting the substrate, data on out-of-plane movements are obtained.

Manual stereoscopy has most often been used to analyze the image pairs (1-4). A trained observer can measure displacements of ± 10 μm between the micrographs, equivalent to ± 2 nm displacement sensitivity at 5000X. Another way to determine the differential displacements from pairs of SEM or optical micrographs is to use digital image processing techniques. We have developed a computer controlled imaging system that determines differential displacement field maps. Termed HASMAP, for High Accuracy Strain MAPper, it is the cornerstone of our experimental mechanics capability and provides the possibility of measuring strain over sub-micron gauge lengths with displacement sensitivity of ± 1 nm. HASMAP calculates the displacement field by comparing the positions of small windows surrounding identical features (texture, surface artifacts, etc) in each micrograph. The calculation of differential displacement is done by a two-dimensional cross-correlation applied to each pair of digitized images. A detailed description of HASMAP is given in Ref. 5, with examples of applications in Ref. 6.

Our ambitious goals for the program were to measure displacements with 1 nm resolution over a 50 nm spatial scale. While we have surpassed the original anticipated accuracy of the displacement measurements, we have not met the desired spatial resolution because the minimal surface contrast of the epoxy resin makes it impossible to identify fine natural features for stereoimaging comparison. We have found it necessary to decorate the surface with MgO particles which limits the spatial resolution in these measurements to 100-250 nm. When measuring displacements of individual decorative particles, manual stereoimaging was found to be more versatile and quicker than the automated HASMAP system. Manual analysis is also much more forgiving of the "shot noise" that appears in SEM micrographs than is HASMAP. The final result is that we achieved adequate sensitivity to measure displacements at very low fiber loads (so as not to damage the fiber/matrix interface), but we could not achieve fine enough spatial resolution to directly measure interphases less than 0.25 μm thick. Fortunately, one should still be able (with appropriate models) to assess the properties of small interphases from measurements made on the local deformation behavior.

3.0 EXPERIMENTAL DETAILS

3.1 Material and Sample Preparation

All samples were supplied by Dr. John Williams, the original program manager at NADC, who later moved to Michigan Technological University. The resin was Epon 828 (100 pt wt) cured with the stoichiometric weight of meta-phenylene diamine (15.5 pt wt). Both the resin and amine were taken from single production batches, the resin being commercial grade material and the amine laboratory grade. The resin was weighed, preheated to 100°C, and mixed with the appropriate amount of solid amine. The mix was stirred thoroughly, reheated to 100°C, and remixed. This ensured that all of the amine melted and was completely dissolved. All of the specimens were cured above 70°C and were exposed to at least 1hr at 100 °C.

The fiber was commercial carbon fiber, Fiberite AS-4, purchased from Hercules in the surface-treated (oxidized, unsized) condition, although two samples used fiber supplied in the coated condition with an epoxy compatible size. One sample of surface-treated fiber was coated with a resole phenolic resin (Karbon 941 from Fiberite). The sample numbers, fiber condition and applied fiber strain at which the data were obtained are given in Table 1.

A single carbon fiber was threaded through the upper and lower holes of the C-clamp tensioning device shown in Fig. 2 and bonded in place. A micropositioner was used to ensure that the fiber was centrally placed in the upper hole. After the resin was fully cured the fiber was cut at the upper surface with a sharp razor blade. The samples were then shipped to the Science Center for displacement measurements.

A flat surface at the fiber/matrix interface was desirable both for the displacement measurements and to match the displacement modelling. A manual polishing sequence was developed to produce such surfaces in the vicinity of the fiber. This entailed an initial polish of the sample on 4000 grit SiC paper, followed by extended polishing on a felt wheel loaded with a slurry of MgO (50 nm). This final polish was repeated to remove small amounts of material in steps until the fiber was exposed and a flat fiber/near-interface region was obtained. Various forms of surface decoration to enhance the contrast of the resin in the near fiber/matrix interface region were tested. We tried an MgO flash, rubbing the fiber region with a soft graphite pencil to leave small patches of graphite on the resin, rubbing the fiber region with a q-tip to scratch the resin, and

Table 1
Tested Samples

Sample #	Fiber	Strain	Temp	Loading Device
6	UC	0.6%	amb	Mechanical system
22c	Phenolic C.	0.4%	amb	Mechanical system
23	UC	0.4%	amb	Mechanical system
24	UC	thermal	cycled	
25	UC	0.4%	cycled -70°F to 160°F	Mechanically loaded after thermal cycles
27	UC	0.24%	amb	PZT system
M37	UC	0.094%	amb	PZT system
M38	Sized	0.084%	amb	PZT system
M39	Sized	0.4%	amb	Mechanical system
M40	Hydrogen'd	0.13%	amb	PZT system
M41	Hydrogen'd	0.4%	amb	Mechanical system
M51	UC/PC	0.13% 0.22%	amb	PZT system
M42	Sized	0.161% 0.100% 0.128%	amb	PZT system

* UC   -   uncoated AS-4 fiber
  Hydrogen'd   -   hydrogenated AS-4 fiber
  amb   -   ambient
  PC   -   Post cured
  Samples 6-28 -   oven cured - no amine environment.
  M series   -   amine environment controlled, made at MTU

evaporating a water-based solution of MgO particles on the surface. The latter procedure worked best. Finally, the specimen was given a 5 nm gold coat to prevent charging in the SEM.

3.2 Mechanical Loading Fixture

Displacements near the interface of a single fiber embedded in an epoxy matrix were measured while the fiber was placed under tensile load using the C-clamp frame designed and built by NADC (Fig. 2). A tensile load was applied to the fiber by expanding the mouth of the fixture using a #2-56 screw.
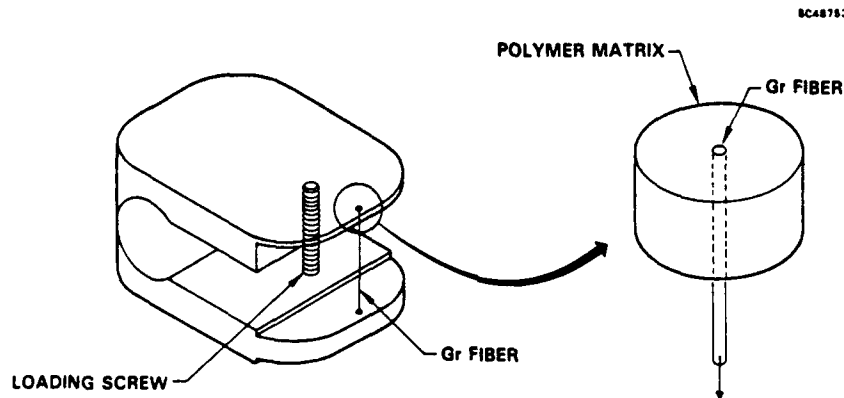
Fig. 2 C-clamp fiber tensioning frame.

The C-clamp load frame was modified to ..;ount onto an existing drive screw in our SEM so that the fiber could be loaded in-situ (Fig. 3). The #2-56 loading screw was driven by a worm gear which was in turn driven by a small vacuum-rated stepping motor attached directly to the base of the mount. The C-clamp tip displacement was very small even at a high fiber strain, ε_f, of 0.5% ($\sim 40\ \mu m$). The system achieved an opening displacement of 4.3 μm/drive shaft turn, with the drive shaft driven by a 12,800 step/revolution stepping motor through a 2:1 gear reduction. The absolute accuracy of the change in opening displacement of the C-clamp tip was $\pm 0.5\ \mu m$, set primarily by the backlash in the worm gear. This self-contained loading package was bolted directly to the tilting stage of the SEM, providing rigid and accurate loading while maintaining maximum flexibility in viewing angle. This mechanical fixture was used for high loads, i.e., $\varepsilon_f \geq 0.4\%$, where the out-of-plane displacements were in the range of 10 to 50 nm. The procedure required taking one micrograph at zero load and one after loading, with about a 4 minute time lapse to obtain the load. The time lapse allowed for small electronic drift in the SEM which produced some magnification change between micrographs. This magnification error was the largest inaccuracy in the displacement measurement. It was minimized by analyzing out-of-plane displacements perpendicular to the tilt axis of the specimen. This provided a displacement sensitivity of ± 2 nm for the mechanical load fixture.

3.3   PZT Loading Fixture

Elastic measurements at low load required that very high accuracy be achieved because the anticipated out-of-plane displacements would be in the 1 to 10 nm range. One way to eliminate the
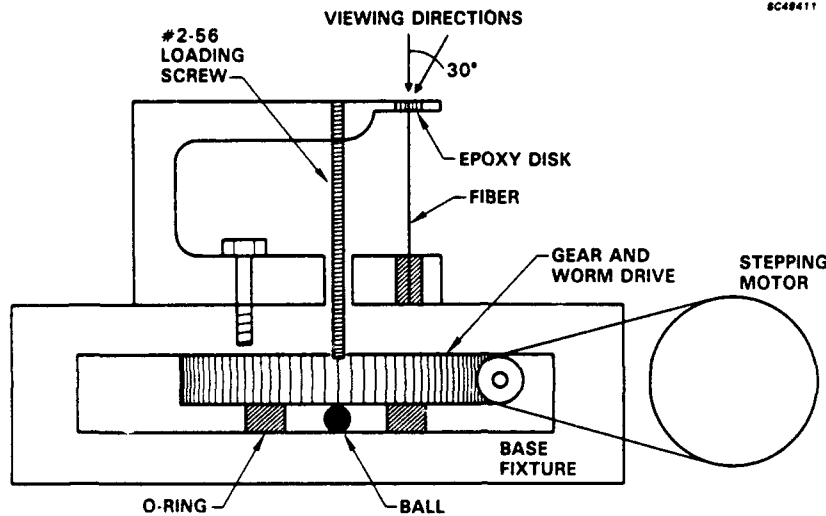
Fig. 3 Diagram of in-situ loading frame.

error from magnification drift is to record both the unloaded and loaded state on one micrograph with little time lapse between the two conditions. This was done by using a piezoelectric transducer (PZT) to instantly load the fiber by application of a voltage which causes the PZT to flex. Using the same C-clamp frame (without the #2-56 loading screw inserted), the PZT was bonded to the fiber about 1 mm below the epoxy disk (Fig. 4). As the micrograph was being recorded, the voltage was applied and the fiber loaded in less time than one scan line on the micrograph (Fig. 5). Fiber strain was controlled by the amount of voltage applied to the PZT. Not only was the magnification drift error reduced, but the technique also eliminated the indeterminate relative rotation between the before and after micrographs. Sensitivity was doubled by recording one micrograph while switching from an unloaded to a loaded state, and a second that was switched from a loaded to an unloaded state. Displacement sensitivity of ±0.5 nm for out-of-plane and ±0.3 μm for in-plane measurements could be achieved, as determined by replicate measurements on 10,000X micrographs. All data was taken at this magnification unless otherwise specified.

It must also be pointed out that pulling directly on the fiber provides a more accurate measurement system than opening the mouth of the C-clamp. The latter produces small but finite rotation of the fiber/matrix surface relative to the electron beam, resulting in a possible parallax error. Although a measurement procedure, described later, was developed to minimize this error for the mechanical loading fixture, direct loading of the fiber via the PZT eliminated all corrections for rotation and parallax.
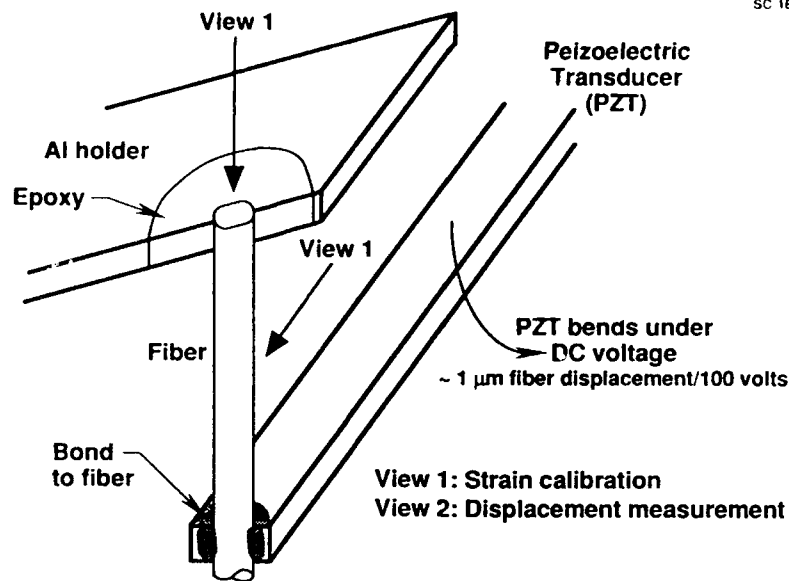
Fig. 4   Diagram of PZT attachment showing the two different viewing angles for strain calibration and displacement measurements.
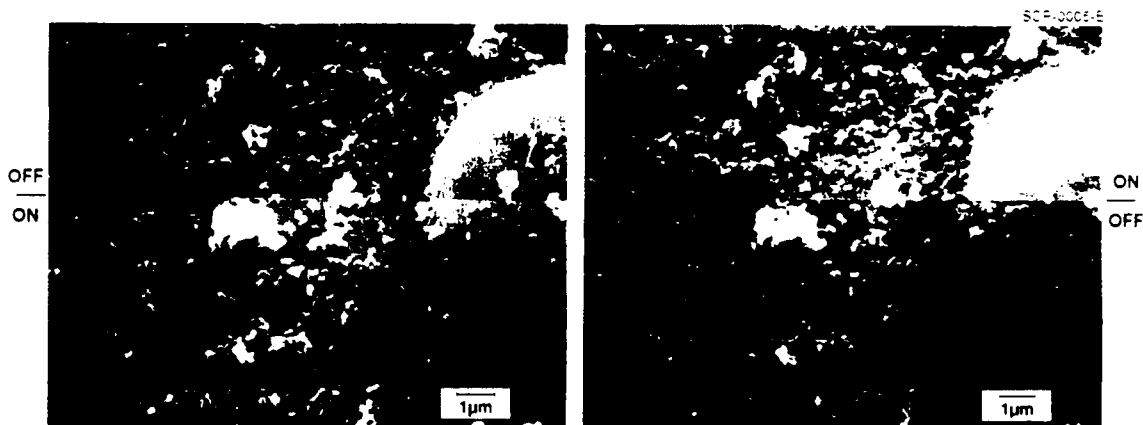
Fig. 5   Micrograph arrangement for PZT system showing displacement measurements along switching line from two micrographs switched oppositely.

3.4   Thermal Loading Fixture

For thermal expansion measurements, the C-clamp specimen was bolted to a resistance-heated aluminum substrate. The temperature was maintained by an external controller connected to

a thermocouple attached to the C-clamp frame. The unit could be freely tilted to achieve the desired viewing angle for in- and out-of-plane studies.

3.5 Measurement of Fiber Strain, ε_f

After curing the epoxy and cooling to room temperature, the AS-4 fiber was left unloaded in the C-clamp fixture. To set the #2-56 loading screw to the zero load point, and to calibrate the subsequent fiber strain, we fabricated a device to enable optical measurement of the strain in the fiber while it was being loaded. Optical micrographs of the side of the fiber were recorded during loading and ε_f measured by stereoscopic analysis of the micrographs. Once the zero load point is found, each additional turn of the drive shaft on the SEM loading frame produced a strain of 5×10^{-3}, equivalent to a fiber load of 0.0045N.

A similar approach was used for the PZT loading system except that the calibration measurement was made in the SEM using PZT loading. A typical calibration curve is shown in Fig. 6.
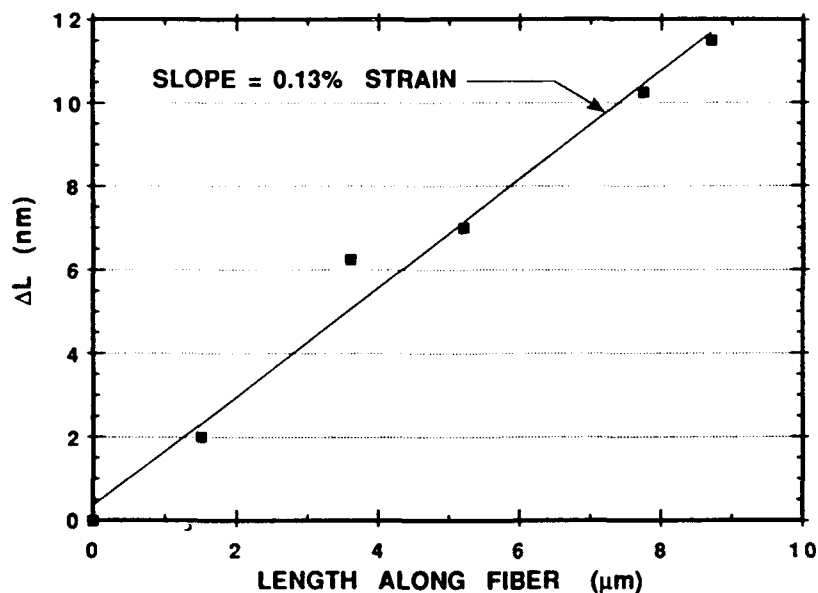
Fig. 6   Calibration curve for PZT loading system for sample #51 at 600V. Slope of cumulative differential displacement vs position along the fiber gives the induced strain on the fiber at the applied voltage.

3.6 Displacement Measurements

The highest resolution displacement measurements were made along a single radii across the fiber along the line C-C' (i.e., parallel to the axis of rotation of the mechanical loading system, and along the ON/OFF switching line for the PZT system), as in Fig. 7. The out-of-plane displacements along C-C' are then measured normal to the rotation axis for the mechanical system. Thus, if the in-plane displacements are radially symmetric, or at least small, the measured displacements are only due to out-of-plane movements and no correction for in-plane movement is necessary. In addition, since we are measuring displacements normal to a common line, the out-of-plane displacements found along the line C-C' are less sensitive to magnification drift. In Fig. 7, no left-right motion of B relative to A can occur for linear changes in magnification.

SC49519

C'

OUT-OF-PLANE MOVEMENT

B

D

A

FIBER

C

ROTATION AXIS
AND DEFLECTION AXIS
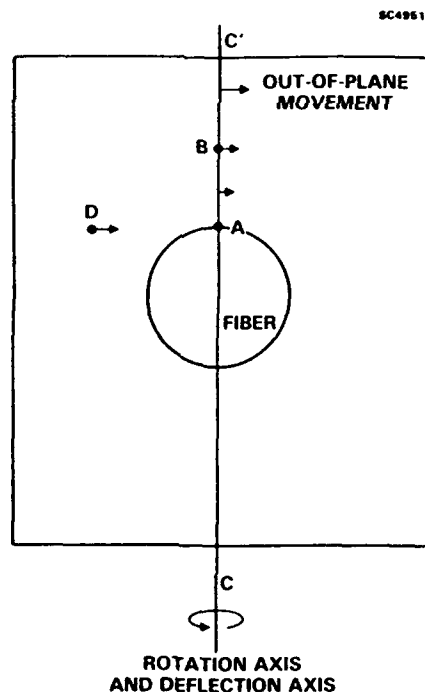
Fig. 7 Radius across fiber shows locus of out-of-plane displacement measurements. Symmetric deformation around the fiber produces only radial in-plane deformation when viewed at a normal angle. Even with tilt, circumferential displacements (i.e., perpendicular to radial) along C-C' (the axis of rotation) are only from out-of-plane movements. Because the circumferential distance between points A and B is zero, changes in magnification cannot effect the measured circumferential displacement. At point D, the in- and out-of-plane movements are mixed and the distance D-A depends on magnification.

4.0 FINITE ELEMENT ANALYSIS

An elastic finite element analysis of the expected deformation was made to assess the magnitude of the displacements, and to determine the depth of the plane strain state. An anisotropic two-dimensional model of the fiber/matrix system was analyzed using ABAQUS. The finite elements were fully orthotropic and modeled a single fiber imbedded in a disk shaped matrix. One half of the radial disk segment was modeled, having an embedded fiber and reflection symmetry across the disk. The material parameters required for radial symmetry are given in Table 2 for the fiber/epoxy system.

An interphase region of 0.5 μm was fixed for all analysis, and calculations were made for various ratios of the interphase modulus to the matrix modulus, E_i/E_m. Typical displacements for $\varepsilon_f = 0.24\%$ are shown in Fig. 8. The out-of-plane displacement, U_2, is given in absolute magnitude, that is, relative to the unloaded surface. Typical displacement of the fiber is 70 to 75 nm for this load. The stereoimaging measurements are differential and give only the relative change from any fixed point, e.g., the surface of the fiber. The ordinate in Fig. 8a can be slid up or down to match the experimental out-of-plane data as long as the scale is not adjusted. While the in-plane displacements, U_1, are smaller in magnitude than U_2, the variance with E_i/E_m ratio is almost as large (Fig. 8b), making it useful to measure both quantities.

Table 2

Material Parameters

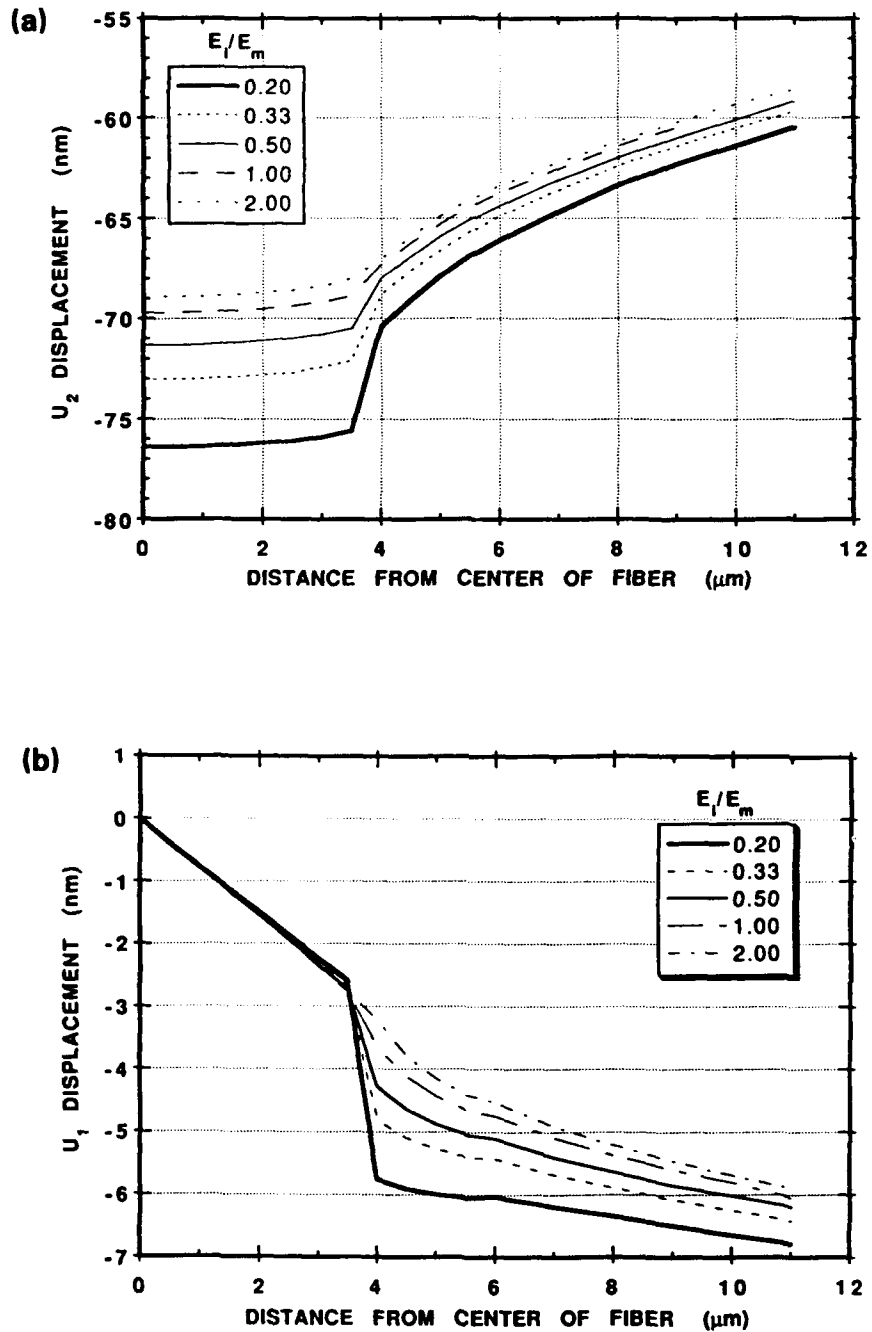| FIBER		
Thermal	α_r	1.3×10^{-5}
Expansion	α_z	0.0
Coefficient (/°C)		
Elasticity	D_{1111}	6.07
Parameters	D_{1122}	2.37
(GPa)	D_{2222}	236.0
	D_{2233}	1.84
	D_{3333}	6.07
	D_{1212}	22.0
	D_{1313}	0.0
	D_{2323}	0.0
MATRIX		
Thermal	α_r	4.0×10^{-5}
Expansion	α_z	4.0×10^{-5}
Coefficients		
(/°C)		
Elasticity	E_z	3.39
Parameters	E_r	3.39
(GPa)		

(a)

(b)

Fig. 8   Displacements calculated from FEM using material parameters in Table 2 and an interphase thickness of 0.5 μm.

5.0 RESULTS

5.1 Elastic Near-Interface Deformation

Low load measurements of U_2 conducted with the PZT load system are shown for the uncoated fiber samples and a sized fiber in Fig. 9, and a hydrogenated fiber in Fig. 10. The displacement data are plotted versus distance from the center of the fiber. The fiber/matrix boundary is at $r = 3.5$ μm in all similar graphs. The measured U_2 displacements and FEM calculations have been normalized to $\varepsilon_f = 0.1\%$ by scaling the displacements by the ratio of the applied ε_f to 0.1% so that they could be compared. Such scaling is valid as long as the displacements are elastic. While the data exhibit a fair degree of scatter on this scale, the actual standard deviation from the $E_i/E_m = 0.5$ calculated displacement is only 0.704 nm. This is very close to the optimum accuracy of ± 0.5 nm, the slight difference resulting from focus changes between the reference and second micrograph. Two separate sets of displacement measurements were made on sample #51 with about the same scatter between sets as for all samples in Fig. 9. Within this scatter band, no difference between the uncoated and the sized fiber can be detected. (Additional sized fiber data can be found in Fig. 18a.) The best predicted fit from the FEM analysis is for $E_i/E_m = 0.5$, although other values between 0.5 and 1.0 may be just as good. A careful statistical fit of interphase models to the data is needed to really assess if the sized fiber displacement data indicate a soft interphase. However, the $\varepsilon_f = 0.24\%$ uncoated data are probably not elastic and should be included in such an analysis.

The hydrogenated fiber sample (Fig. 10) shows a distinctly softer interphase in that the U_2 displacements are larger and the best fit modulus ratio is $E_i/E_m = 0.20$. Note especially the data point at $r = 11.2$ μm is far greater than any in Fig. 9. However, hydrogenated sample M41 exhibited interphase cracks when loaded to $\varepsilon_f = 0.4\%$. Such gross damage suggests that the 0.13% fiber strain data may not be elastic.

In-plane displacement measurements are compared to FEM calculations for an uncoated fiber (Fig. 11) and a sized fiber (Fig. 12). The data are presented at their measured fiber strain to show the significant difference in displacement at higher loads. While the U_1 displacements at comparative loads are smaller than the U_2 displacements, the relative accuracy of the displacement measurement is improved. Even so, one cannot easily differentiate between the various E_i/E_m ratios any better than with the U_2 data.

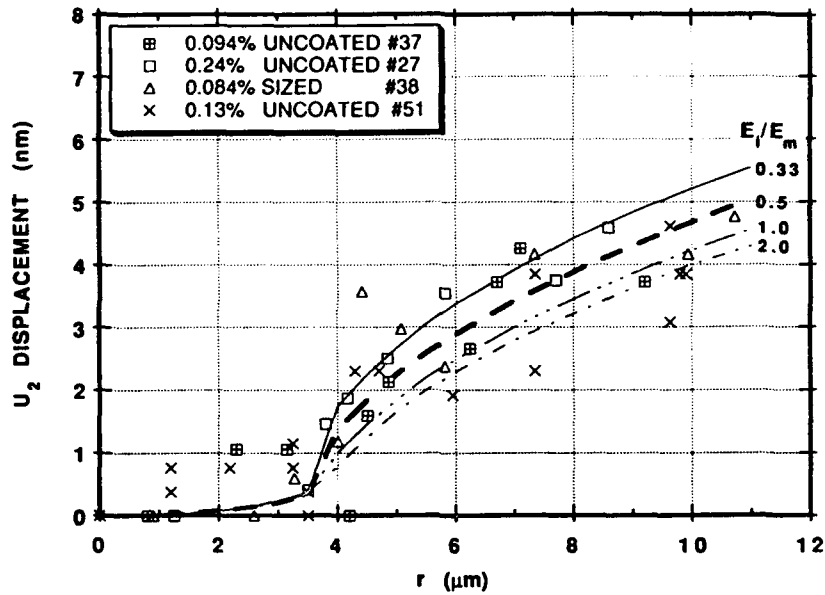Fig. 9   Out-of-plane displacements for samples loaded in the elastic regime Data scaled to
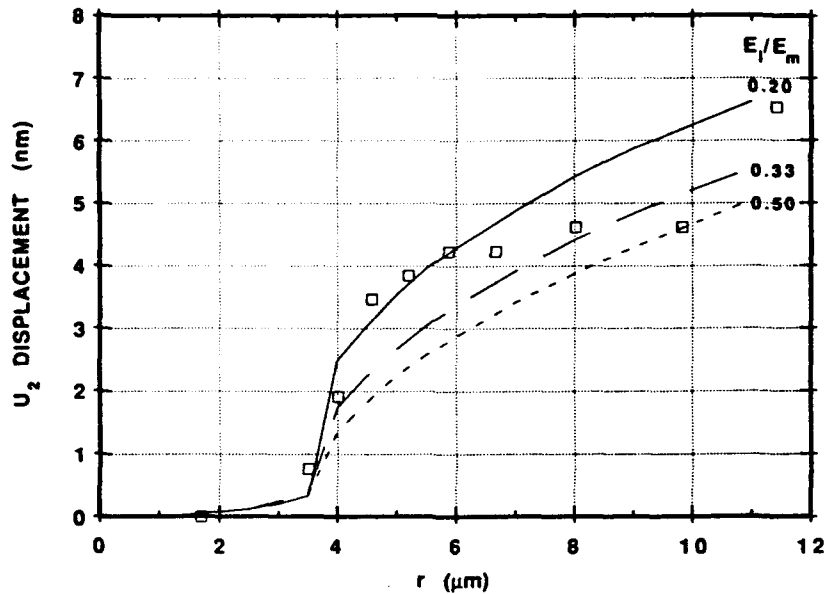$\varepsilon_f = 0.1$ %.

Fig. 10   Out-of-plane displacements for hydrogenated fiber sample loaded in the elastic regime
to $\varepsilon_f = 0.13\%$.

15
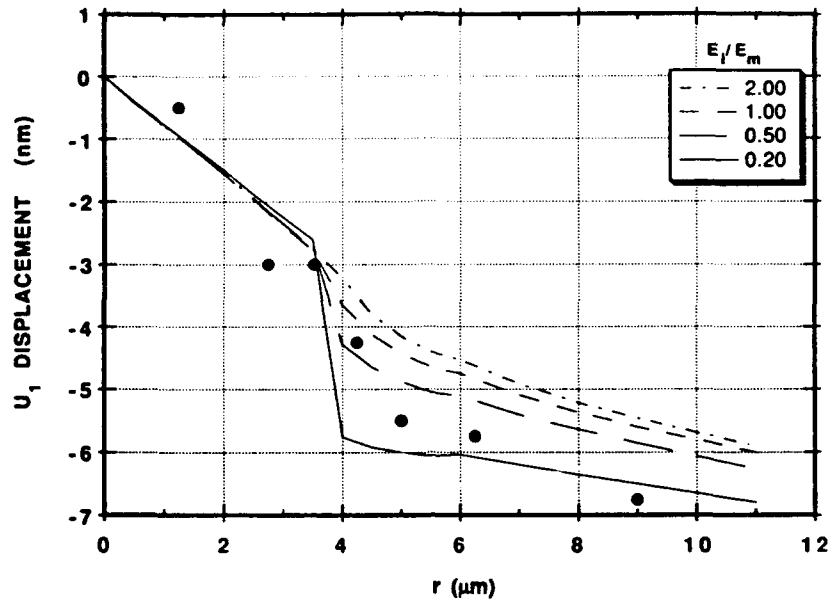
Fig. 11 In-plane displacement of uncoated fiber loaded to 0.24% fiber strain.
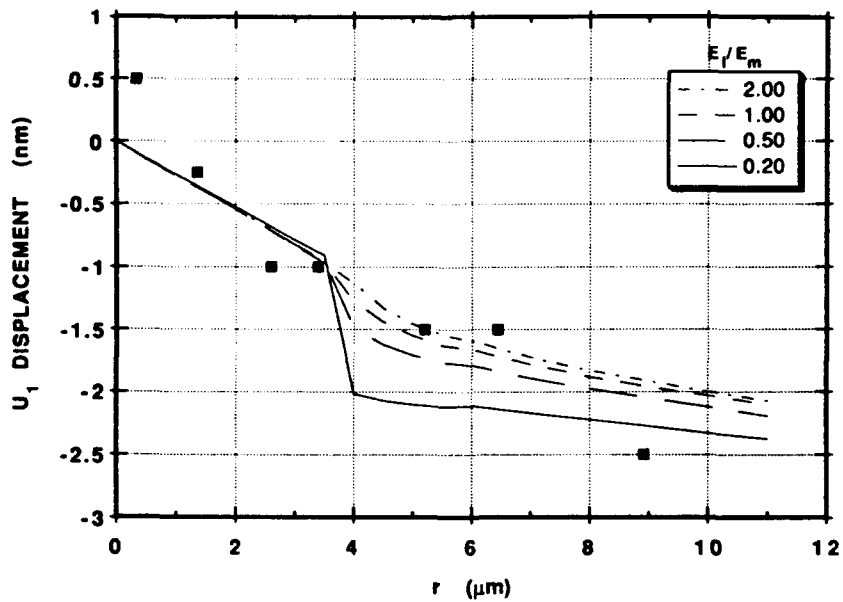
Fig. 12 In-plane displacement of sized fiber loaded to 0.084% fiber strain.

Elastic out-of-plane data for the phenolic coated sample is shown in Fig. 13 and compared to the FEM calculations. The data (square symbols) were taken using the mechanical load system at $\varepsilon_f = 0.4\%$. This sample shows much less displacement than for all the other samples indicating either a stiffer or a much narrower interphase than used in the FEM. But, there is an interpretive problem here because unlike the PZT system, having loaded and unloaded views on different micrographs for the mechanical loading system introduces an indeterminate rotation angle. The triangles in Fig. 13 are an equally likely value for the data obtained by correcting the original data for the slope in the fiber.
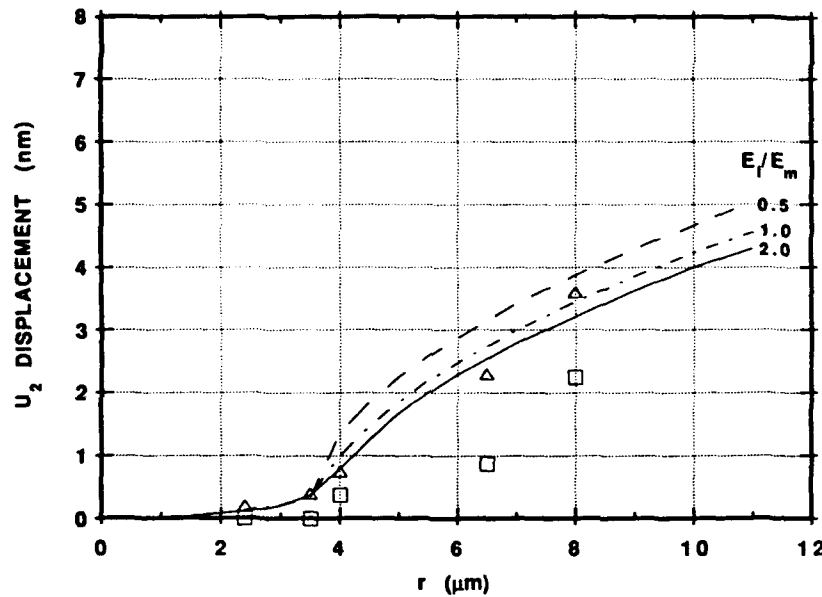
Fig. 13   Out-of-plane displacements for the phenolic coated sample loaded to $\varepsilon_f = 0.4\%$, which was still in the elastic regime for this sample. Scaled to $\varepsilon_f = 0.1\%$.

5.2   Transient Near-Interface Matrix Deformation

During development of the displacement measurement technique with the mechanical loading fixture, data were taken at $\varepsilon_f > 0.4\%$. The data exhibited an inelastic behavior which changed with continued load cycling. This transient out-of-plane displacement result was documented over the first load cycle for specimen #23 (uncoated AS-4 fiber). Upon application of

a tensile load to the fiber, the matrix near the interface fell relative to the fiber (Fig. 14a). Not only does this offset increase with applied load, it increases further during the unloading portion of the load cycle also (Fig. 14b). The distance from the interface of the maximum difference in height between the matrix and fiber progressively increases with matrix shrinkage. After unloading, it lies about about one fiber radius from the interface. Comparing the micrographs taken at zero load before and after the single load cycle, the maximum residual displacement is 0.3 μm. The deformation is clearly nonuniform as the cross sectional values in Fig. 14 show. A full topographical plot of the mixed in- and out-of-plane displacements (Fig. 15b), obtained by comparing micrographs of the unloaded surface taken before and after a full load cycle, shows the variation in height change with location. The largest drop in matrix height relative to the fiber surface is that of the 0.3 μm contour on the left side of the fiber. This corresponds to the dip seen on the left side of the fiber in Fig. 14b.

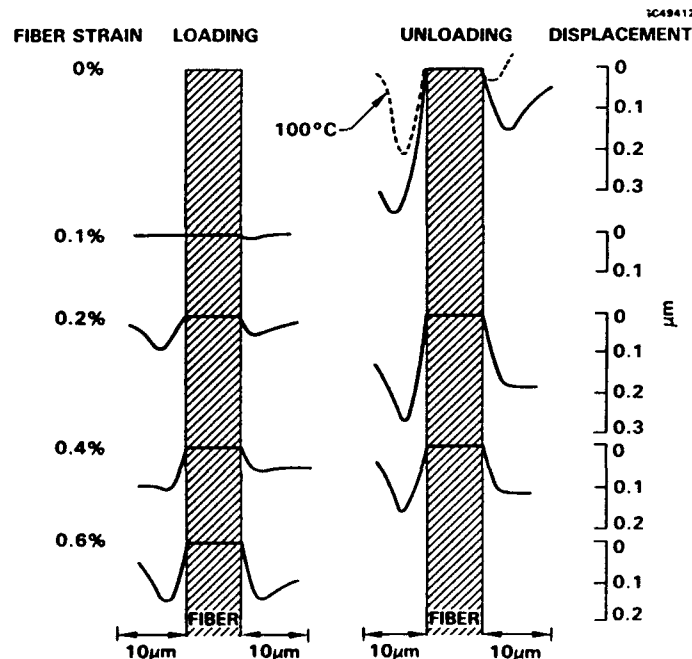Fig. 14   Out-of-plane displacements of matrix relative to fiber along a radial line across the fiber. Diagram follows progression through the first complete loading and unloading cycle.

SC49413

UNLOADED MICROGRAPH

ISO-DISPLACEMENT CONTOURS
AFTER ONE LOAD CYCLE

(a)

(b)
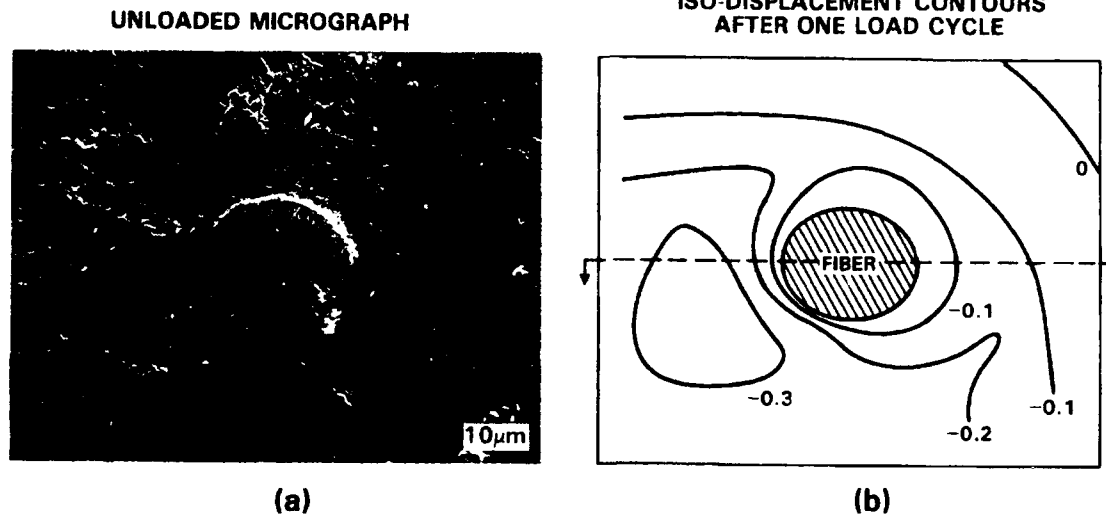
Fig. 15 (a) micrograph of fiber and matrix showing analysis region, (b) topographical map obtained using HASMAP showing contours of U_2 displacement in steps of 10 nm.

To assess possible creep effects in the vacuum environment, the specimen was left in the SEM under vacuum for 24 hours after returning the fiber to zero load. No further deformation took place over this time period. The C-clamp frame was then transferred to a heating stage and heated to 100°C, the original curing temperature. Substantial recovery of the vertical displacement occurred on heating except in the region of the deepest offset. Subsequent polishing of the specimen surface revealed a shallow subsurface crack on this side of the fiber (Fig. 16) located about 0.7 μm from the interface. Noting the largest vertical offset in Fig. 14 did not recover after heating, it appears likely that the deformation during unloading resulted from cracking of the matrix.

We had seen similar near interface deformation patterns in three previous samples, and had indications that the net out-of-plane displacements reached nearly constant magnitude after cyclic loading. This behavior was verified with sample #23 used for Fig. 14. After polishing to remove the near surface damage, including the crack seen in Fig. 16, the fiber was reloaded several times to 0.4% strain. With each reload, the displacements within a few microns of the interface decreased and finally ended up above the fiber. Non-elastic deformation was still apparent at distances more than 3 μm from the interface.

SC49682

Fig. 16   Micrograph of fiber from sample #23 after polishing. A circumferential crack is revealed in the lower left of the fiber.

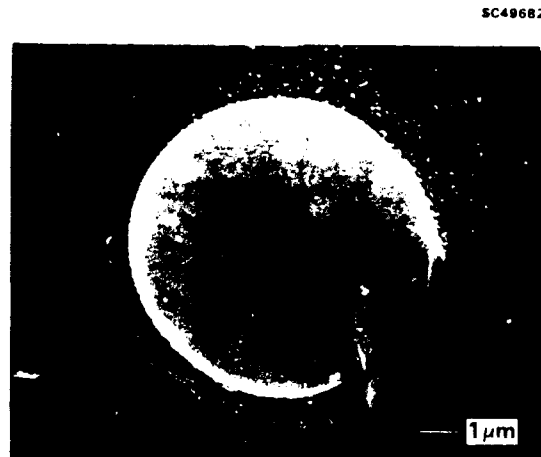The transient dip clearly involves at least two phenomena: 1) near-interface microcracking on unloading, and 2) permanent shrinkage of the matrix. Some of the microcracking is very localized near the surface, and in this experiment about 0.7 μm from the interface. While the thickness of material removed to eliminate the near interface was not critically measured, it was on the order of a few microns. The cause for the near-interface shrinkage of the matrix is open to speculation, but we believe it involves relaxation on tensile loading of the fiber of the longitudinal tensile residual stresses produced in the matrix by the differential thermal expansion between the fiber and the matrix on cooling from the cure temperature (see ζ6.3).

Several additional experiments give this hypothesis credence. No creep takes place in the unloaded state. With load, creep was observed in sample #6 held at $\varepsilon_f = 0.5\%$. The creep rate was maximum on loading and decreased essentially to zero after 8 hours. Several subsequent loading and unloading excursions produced only modest change in matrix height until a single unloading cycle caused a sudden and large displacement, probably due to an interface crack. The specimen was different from that used in our other experiments in that the thickness of the matrix disc was ~ 500 μm instead of the usual 150 μm. This allowed for a large differential thermal expansion on cooling from cure, and hence a potentially greater relaxation displacement.

5.3   Hysteresis Measurements

Due to this transient inelastic deformation, all samples analyzed at $\epsilon_f > 0.25\%$ using the mechanical loading fixture were pre-cycled at $\epsilon_f = 0.6\%$ before preparation of the surface. Without cycling, no stable reversible deformation was measurable. This process apparently served to modify the interphase region and decrease the inelastic response. To test that true elastic behavior was being measured after cycling, the displacement/strain response was measured as in Fig. 17. U_2 was measured both during loading and unloading to obtain a hysteresis loop as illustrated in Fig. 17a. The width of the loop at different maximum fiber strains was measured to determine the strain at which elastic deformation was occurring (Fig. 17b). In this way, elastic deformation at $\epsilon_f = 0.4\%$ was verified for both the sized (sample #39) and the phenolic coated sample (sample #22, Fig. 17). Measurements on the uncoated fiber sample #6 showed that even after repetitive cycling, the U_2 displacement behavior was inelastic at $\epsilon_f = 0.4\%$. We now believe that even though the deformation was elastic at 0.4% fiber strain in samples #22 and #39, the precycling badly microcracked the interphases and changed the elastic response.
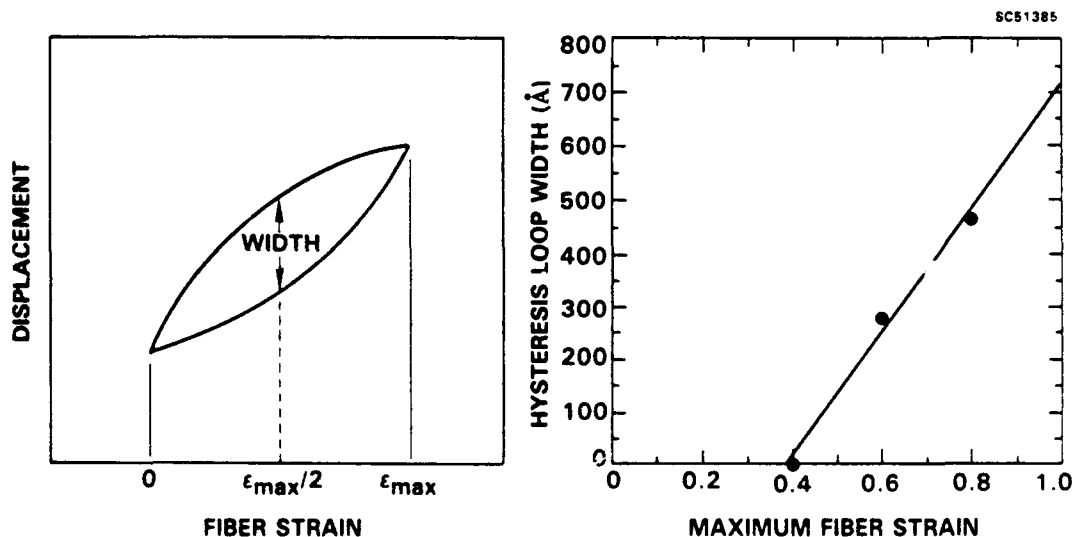
SC51385

Fig. 17   (a) Illustration of hysteresis loop width measurement, (b) Fiber strain for elastic behavior set by zero hysteresis loop width, sample #22.

Sized Fiber Condition: Fig. 18 compares normalized U_2 displacements at five fiber strains for sized fibers. All data less than $\epsilon_f = 0.13\%$ are equivalent and therefore clearly elastic (Fig. 18a). The $\epsilon_f = 0.4\%$ data are also "elastic," but taken after mechanical cycling to reduce the transient effect discussed in $\zeta 5.2$. Substantially different response is seen. The high strain data indicate that the interphase is much softer, presumably having been damaged during high fiber strain cycling. Subsequent microscopic examination conducted at NADC by cross-sectioning the sample showed that a subsurface crack had formed in the interphase region parallel to the fiber which propagated through most of the epoxy disk.

Uncoated Fiber Condition: U_2 displacement data for three fiber strains are compared in Fig. 19 (scaled to $\epsilon_f = 0.4\%$) for uncoated fiber samples. While the data from 0.094% and 0.24% are nearly indistinguishable, the 0.4% data clearly represents a softer interphase. The higher strain level (the sample had experienced $\epsilon_f = 0.6\%$ during cycling to reduce the transient effect) produced a marked change in the interphase modulus.

Coated Fiber Condition: Fig. 20 compares U_2 data from the coated fiber sample #22. The data have been scaled to 0.4% for comparison. The extremely steep jump in U_2 displacement adjacent to the fiber/matrix boundary for the higher strain measurement indicates a large change in modulus of the interphase. Thus, the onset of inelastic response reflects a large change in the effective interphase properties.

Hydrogenated Fiber Condition: In the elastic loading regime, the hydrogenated fiber exhibited the softest interphase. At $\epsilon_f = 0.4\%$, the U_2 displacements were the largest measured, approaching 150 nm at 6 μm from the fiber. However, inspection of the surface revealed an interface crack which broke through the measurement region. The discontinuity thus invalidates the displacement data from which the interphase modulus could be calculated.

Two forms of damage are known to be associated with a change in the interphase modulus, either formation of interphase cracks or relaxation of the transient response of the interphase. The inelastic response of the interphase is significantly affected by the fiber condition. Fig. 21 compares inelastic data taken at $\epsilon_f = 0.4\%$ for three different fiber conditions. For this comparison, the coated fiber data at $\epsilon_f = 0.6\%$ was linearly scaled to 0.4% fiber strain. While this may not be strictly valid in the inelastic regime, it allows for qualitative comparison of the influence

(a)

(b)
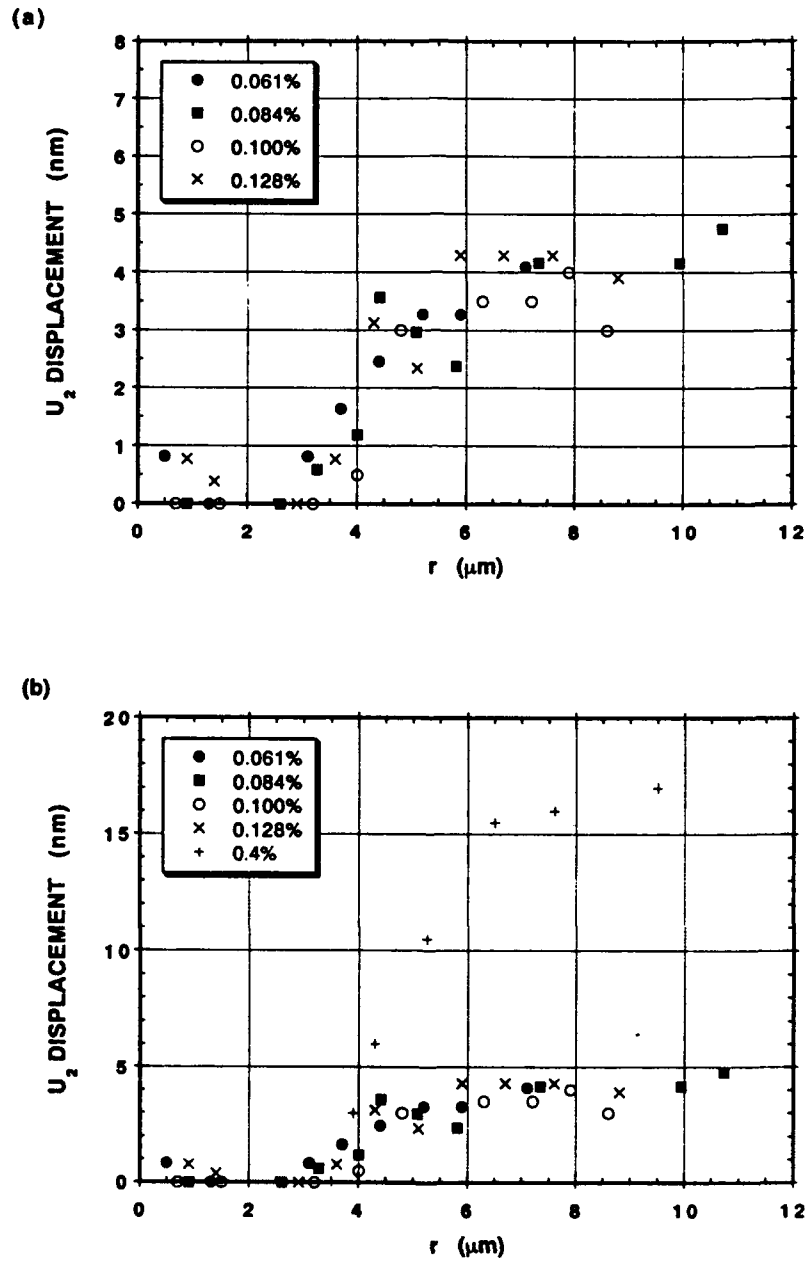
Fig. 18   Out-of-plane displacement for sized fiber samples at multiple fiber strain amplitudes. Data scaled to 0.1% fiber strain for comparison. (a) elastic regime, (b) including high load data.
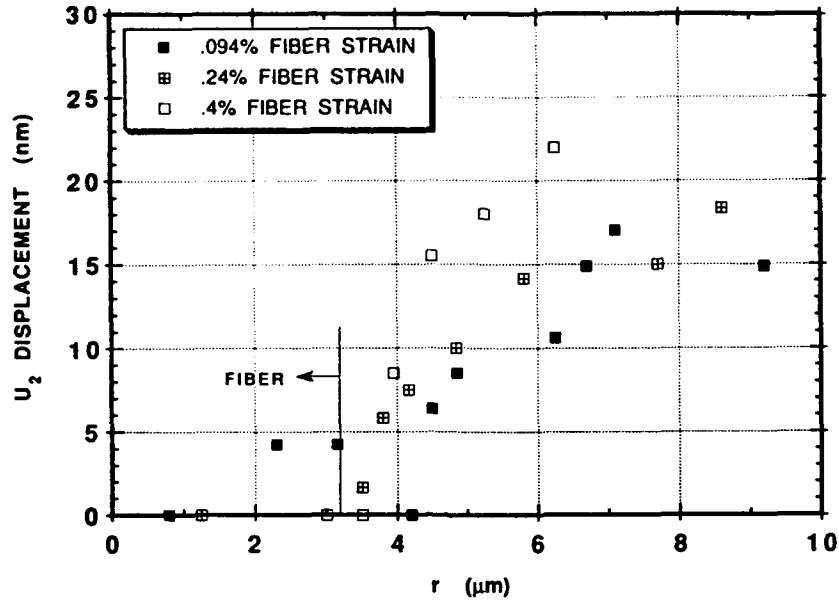
Fig. 19   Out-of-plane displacement for uncoated fiber samples at three fiber strain amplitudes.
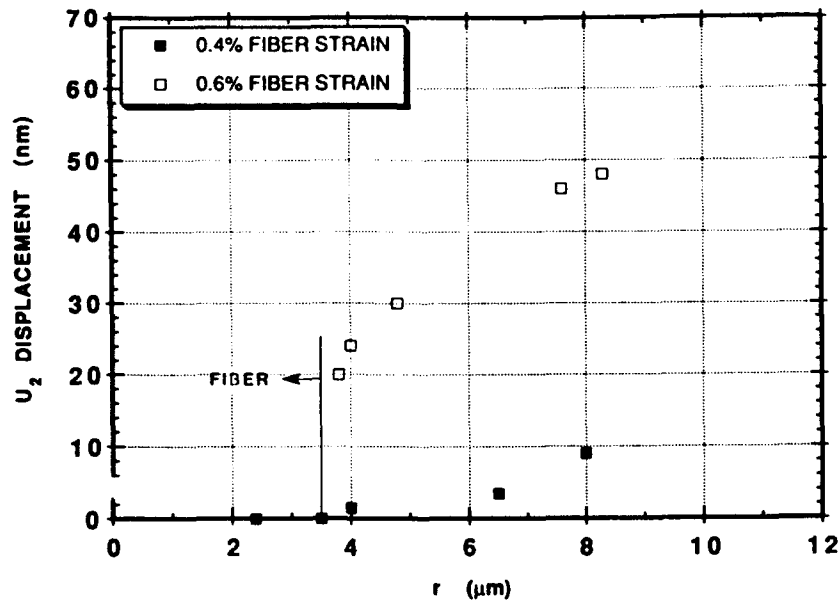Data scaled to $\varepsilon_f = 0.4\%$ for comparison.

Fig. 20   High fiber strain data for phenolic coated fibers. Data scaled to $\varepsilon_f = 0.4\%$ for
comparison.

of the fiber condition. The sized fiber exhibits the softest interphase, most likely due to interphase cracking that was found by sectioning. While both the coated and uncoated fiber show similar U_2 displacements, the uncoated fiber exhibits inelastic effects between fiber strains of 0.24 - 0.4%, while the coated fiber was elastic up to $\varepsilon_f = 0.4\%$.
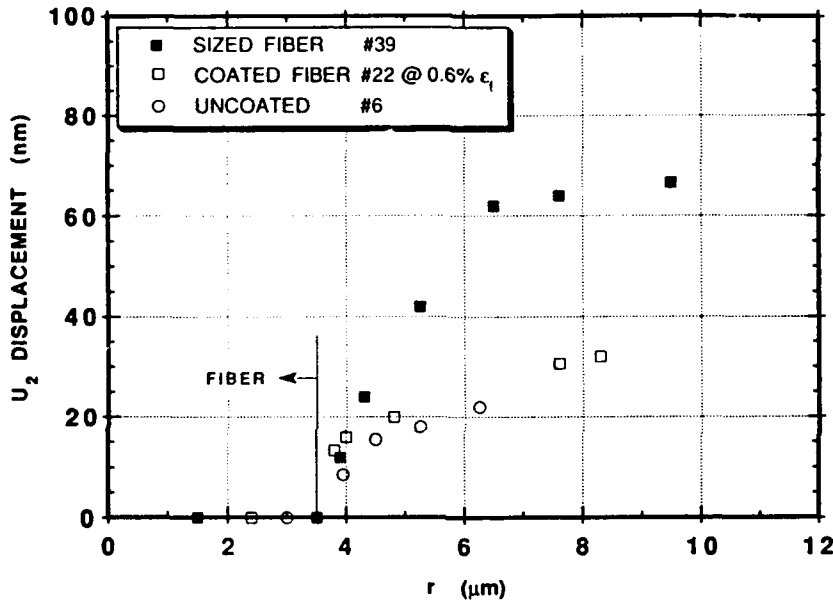
Fig. 21   High fiber strain displacements for different fiber conditions. Data scaled to $\varepsilon_f = 0.4\%$ for comparison.

5.5   Thermal Expansion Experiments

Finite element analysis indicated that substantial in-plane displacements at the interface can be generated by heating, and that the influence of a soft interphase region should affect such displacements. To test this, two samples (specimen #24, uncoated AS-4 fiber, and specimen #22, phenolic coated AS-4 fiber) were heated in the SEM from ~ 35°C to 65°C. Stereoscopic examination of the near-interface micrographs taken at the two temperatures verified that the net strains were compressive on heating. The displacements were not uniform, however. The results in Fig. 22 are for a region judged typical for each case. The data have been plotted after subtraction of a constant sloping background due to the uniform thermal expansion and magnification drift in the SEM. Also, since the high temperature for each sample was slightly

different, the displacements have been normalized by the exact temperature range. A striking difference between the coated and uncoated fiber is evident. The uncoated fiber specimen exhibits much greater in-plane displacement near the interface, suggesting a softer interphase region. A more detailed HASMAP analysis along an entire segment of the interface (Fig. 23) shows that the soft interphase in the uncoated fiber sample is well defined and less than 0.5 μm thick.

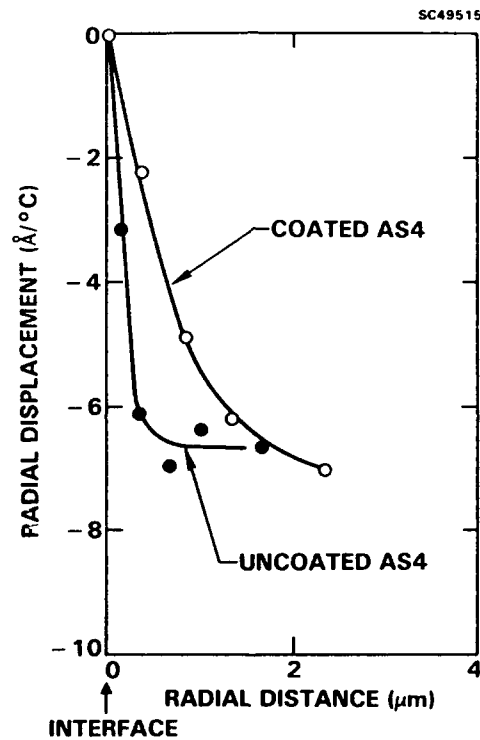Fig. 22 Elastic component of radial displacements from heating.
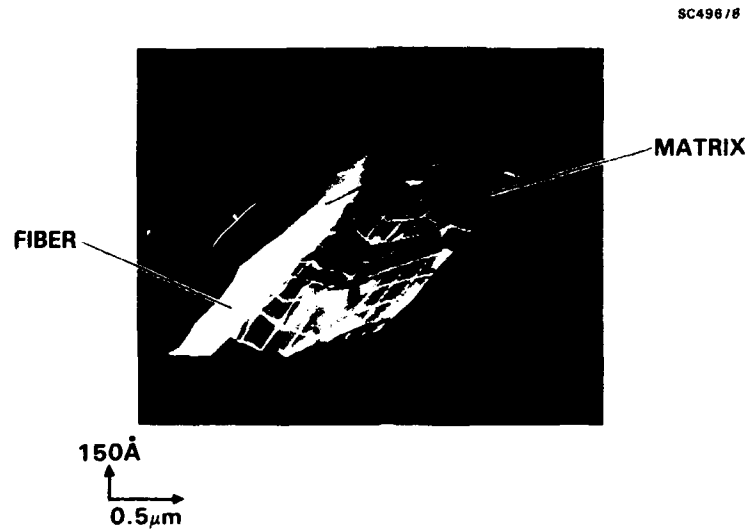
SC496/6

FIBER

MATRIX

150Å

0.5μm

Fig. 23   Perspective view of radial displacements of uncoated fiber produced by HASMAP.
The depression just to the right of the fiber is the interphase in compression.

6.0   DISCUSSION

6.1   Effect of Fiber Surface Treatment on Interphase Properties

Interphase displacement measurements perfect in all regards are not possible given the current state of the art. At high loads where the displacements are of sufficient magnitude to be measured accurately, the deformation is inelastic. In the elastic regime ($\varepsilon_f < 0.25\%$) the displacements are so small it is difficult to differentiate modest differences in the modulus ratio E_i/E_m. Nevertheless, it appears possible that, for the sized fibers, there exists an elastically soft interphase with a thickness in the range of 0.5 μm, whereas no interphase is apparent for the uncoated fiber and phenolic coated fiber samples.

Clearly, at sufficient fiber strains above 0.25%, damage occurs in the interphase which modifies the interphase modulus. The strain at which damage occurs, and the magnitude of damage is dependent on the fiber condition and indicates something about the nature of the interphase. The hydrogenated fiber surface suffers interphase damage at the lowest strain. In Fig. 19, there is some hint that the interphase may be affected as low as $\varepsilon_f = 0.24\%$ for the uncoated fiber, but certainly by 0.4% a large change has taken place. The interphase for the phenolic coated fiber only exhibits an inelastic affect at quite high strains, i.e., $\varepsilon_f = 0.6\%$ in Fig. 20. And Fig. 21 shows that the modified modulus at high strain depends on the fiber condition.

Taken together, these data would suggest that in the elastic regime, the interphase can have only marginal affect on the mechanical properties. However, damage which occurs in the interphase at high strains is very dependent on the fiber condition. While such high shear strains in the interphase are unusual, since in most structural applications both the fiber and matrix are loaded together, once local cracking begins such as from fatigue these interfacial properties can be extremely important.

6.2   Plane Stress-Strain Considerations

For systems in which the fiber and matrix modulii are of comparable magnitude, the plane stress surface layer is thinner than one fiber diameter (typically on the order of nanometers). If the entire fiber/resin system were in plane strain, the single fiber would follow the thermal displacement of the matrix during cooldown from the curing temperature. Relaxation of the

thermal contraction strain could not cause the inelastic response of the interphase measured in this program, but rather would allow the fiber to expand longitudinally.

However, the fiber and matrix modulii in the present problem differ by two orders of magnitude. The finite element model described in $\zeta 4.0$ was used to calculate the longitudinal stress in the fiber, σ_{zz}, induced during cooling. For a temperature drop of 80 °C, σ_{zz} increases with thickness of the epoxy disk as shown in Fig. 24. For the 150 μm thick epoxy disk, σ_{zz} reaches a value of -350 MPa in the center of the disk, substantially less than for the thick epoxy disk. Thus, because of the differing modulii, the entire fiber/disk system is essentially in plane stress for the 150 μm disk thickness. Relaxation of the strain induced from differential thermal contraction would allow the matrix to shrink.

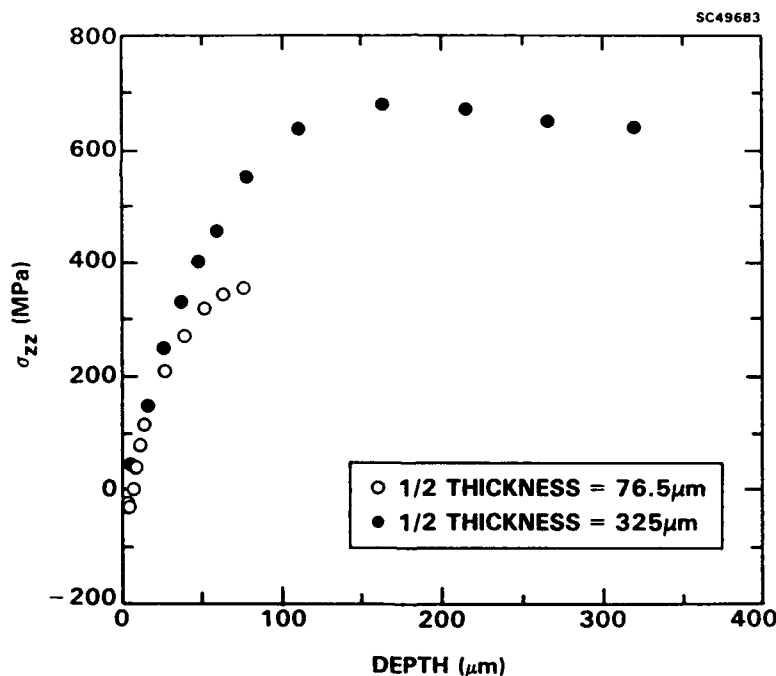Fig. 24 σ_{zz} in the fiber developed by differential thermal expansion for two epoxy disk thicknesses.

On cooling from the cure temperature (100°C), the fiber stresses for the 150 μm thick disk are compressive (except near the surface) and orders of magnitude larger than the balancing tensile stress in the matrix (Fig. 25a). However, the shear stress, τ_{xy}, is of comparable magnitude in

6.3   Explanation of Inelastic Effect

Because the fiber/epoxy system is essentially in a plane stress state, stress relaxation of the interface region can take place. We do not have a model of the actual process of relaxation of the thermal residual strains, and so cannot fully simulate the transient deformation observed. However, we can examine an upper bound to the displacements by allowing the stress state induced from 80 °C cooling to relax completely. The results in Fig. 26 were obtained. To simulate the elastically soft interphase a column of interface elements representing a 1.0 μm thick layer having a modulus one-tenth that of the matrix was added. The model dictates that the relaxation and sliding of the matrix occurs in the interface elements. In reality, the epoxy remains bonded to the fiber so that the maximum displacement is displaced from the interface. Despite this difference, the maximum vertical shrinkage is approximately that measured experimentally for the thick epoxy disk of sample #23 (compare Fig. 26a with Fig. 14). For the thicker epoxy disk thickness (500 μm), the relaxation effect is much larger (Fig. 26b) as was seen in sample #25 (see ζ5.2). Thus, one obvious explanation ofr the transient is that is results from an effective lowering of the interphase modulus due to microcracking.

6.4   Ultimate Measurement Sensitivity

The PZT fiber loading system permits very accurate displacement measurements to be made. The current sensitivity limitation is due to inadequate surface contrast. The deposition of 50 nm MgO particles from an evaporated slurry does not produce a uniformly decorated surface because the particles tend to agglomerate. This limits the points at which displacement data can be obtained, and produces some extraneous results when the particles rotate or shift between the before and after micrograph.

With improved surface decoration, the PZT fiber loading technique and stereoscopic displacement measurement should be capable of providing a measurement sensitivity of ±0.2 nm every 0.1 μm along a radius through the fiber, interphase and matrix. This would reduce the noise associated with the data (e.g., Fig. 18) and allow for better discrimination as to the effect of fiber surface treatment in the elastic regime. It would also give higher resolution on the thickness of any interphase present.

both materials, and especially large near the surface (Fig. 25b). This shear stress may play a role in microcracking the interphase region.

a)

SC49679
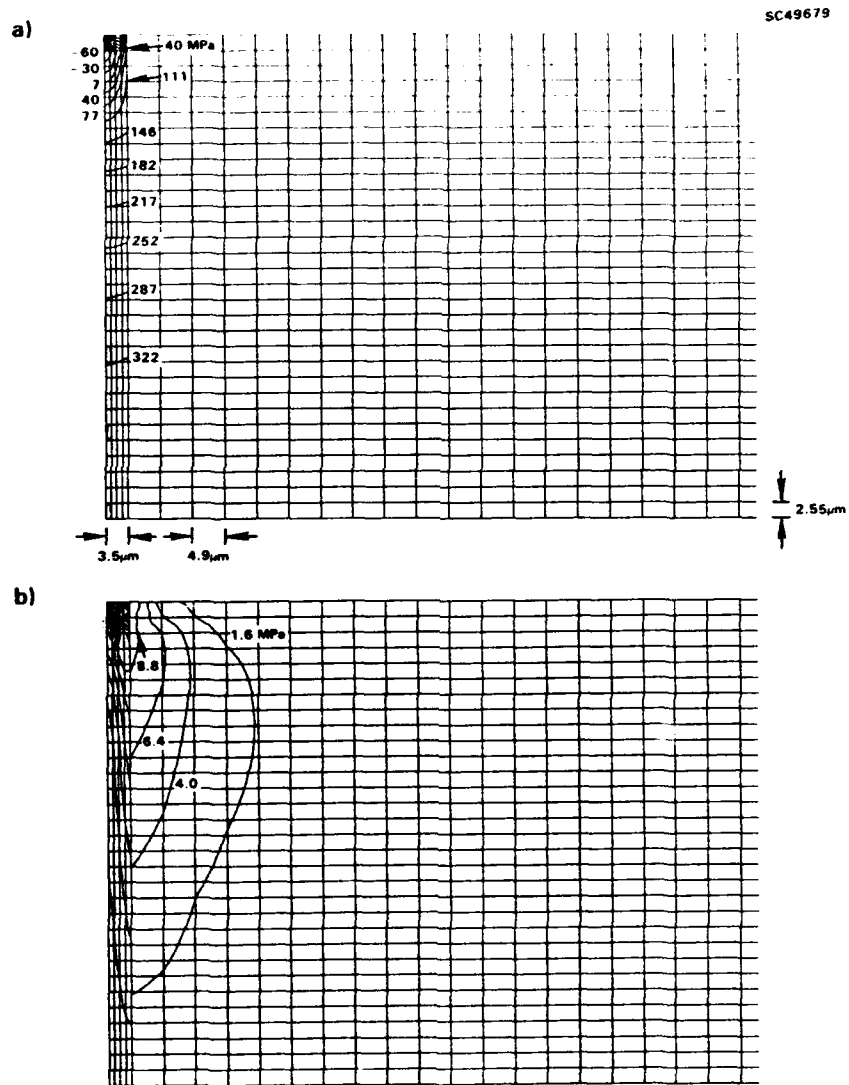
b)

Fig. 25 Stress for the noninterphase case with a 150 µm thick epoxy disk. (a) σ_{zz}, (b) τ_{xy}.

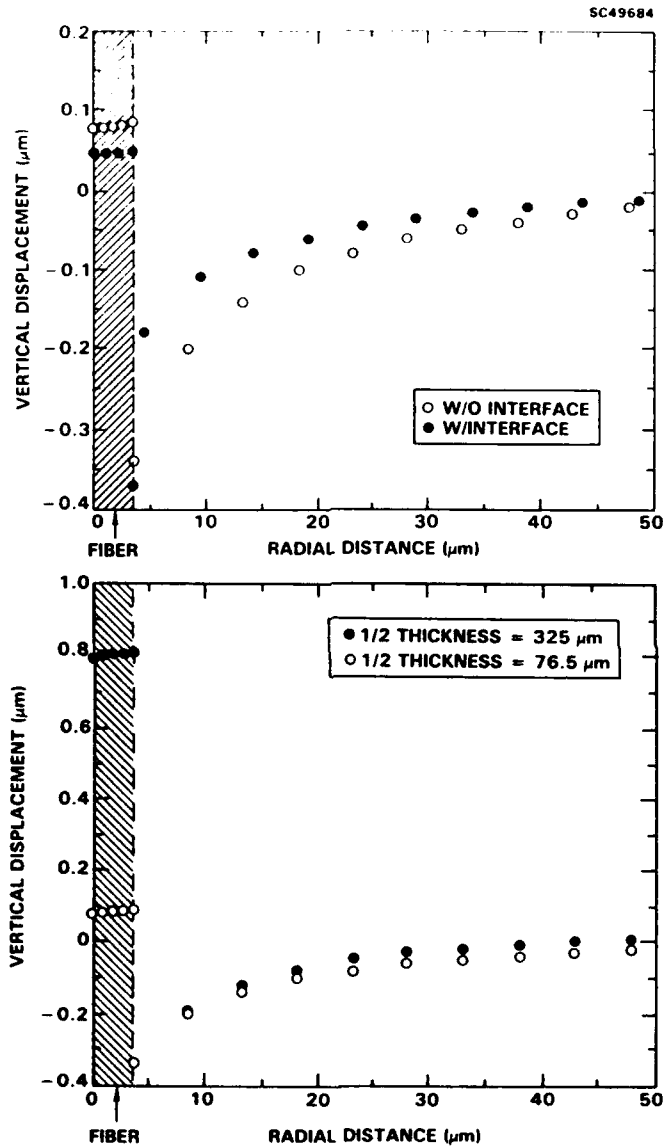Fig. 26   Displacement caused by residual stress relaxation, (a) effect of soft interface; (b) effect of epoxy disk thickness.

7.0 CONCLUSIONS

1 In-plane and out-of-plane displacements of a tensioned fiber/matrix interphase region were measured to an accuracy of ±0.5 nm over a spatial scale of ~ 0.2 μm. The data are of sufficient accuracy for NADC to use to determine the elastic properties of the interphase.

2 Out-of-plane displacements measured at high fiber strains (ε_f > 0.25%) show that the interphase deforms nonlinearly on first loading, possibly by relaxation of the residual strains induced during curing. The transient deformation apparently modifies, or even cracks the interphase thereby lowering the effective modulus. The fiber strain at which the interphase becomes nonlinear is very dependent on the surface treatment of the fiber. The phenolic coated fiber interphase region stays elastic the longest, up to $\varepsilon_f = 0.4\%$, while the sized fiber interphase is softer than the uncoated fiber interphase in the inelastic regime.

3 Regarding questions on the presence of an elastic interphase between the fiber and the matrix, we make the following remarks:

   a. The hydrogenated fiber appears to have the lowest modulus interphase region. However, even at the lowest fiber strains used in the present study, it is possible that this results from microcracking or other damage to the interphase, given the degree of change seen at higher loads.

   b. Data on the phenolic coated fibers were only obtained using the mechanical loading system, leading to some subjectivity as to the exact magnitude of the displacements (see discussion of Fig. 13). An accurate description of the phenolic coated sample displacements from the FEM model shows there is no apparent interphase with this coating. The coated fiber interphase exhibited the highest fiber strain before onset of inelastic deformation.

   c. Low fiber strain data for the sized and unsized fibers are clearly elastic. The PZT loading system allowed for these low fiber strain measurements, and eliminated uncertainties in reduction of the data. Because the strains needed to keep the interphase elastic were a factor of 10 smaller than originally assumed for this program, the displacements are very small and would be unmeasurable without the PZT approach. However, the data are still noisy. Complicating the detection of an interphase effect is the presence of a large, relatively speaking, elastic displacement

at the fiber/matrix boundary even with no interphase modulus difference (Fig. 8). Interpretation of the raw data (Fig. 9) as to which fiber condition produces the softest interphase is prone to subjectivity. A final decision as to the influence of fiber treatment on the mechanical properties of any elastic interphase awaits a careful statistical analysis of these results.

4   While this program concentrated on the influence of fiber surface treatment on the elastic behavior of the interphase, the affect of fiber surface treatment on the inelastic behavior at high load may have more important ramifications. Because the fiber and matrix are jointly loaded in most structural applications, the high shear strains applied in the measurements in this program are not normally experienced by the interphase. But once local crack formation begins such as from fatigue, both the elastic and <u>inelastic</u> behavior we have seen will dictate the ability of the system to resist further damage. Both the interphase stress/strain response and its evolution with cycles will be important to the micromechanics of this damage process and fiber surface/interphase modifications can be expected to have pronounced effect on the structural damage tolerance.

8.0 PUBLICATIONS FROM CONTRACT

1. J. G. Williams, M. E. Donnellan, M. R. James and W. L. Morris, "Elastic Modulus of the Interphase in Organic Matrix Composites," MRS Symposium on Interfaces in Composites, **170** (1989) 285-290.

2 J. G. Williams, M. E. Donnellan, M. R. James and W. L. Morris, "Properties of the Interphase in Organic matrix Composites," J. Materials Science and Engng., **A126**, 305-312 (1990).

3. J. G. Williams, M. E. Donnellan, M. R. James and W. L. Morris, "Elastic and Inelastic Deformation in Organic Matrix Composites," Proc. Fifth Tech. Conf. on Composite Materials, Am. Soc. for Composites, East Lansing, MI, June 10-13 (1990) 127-136.

9.0 REFERENCES

1. B. N. Cox, W. L. Morris and M. R. James, "High Sensitivity, High Spatial Resolution Strain Measurements in Composites and Alloys", Proc. Nondestructive Testing and Evaluation of Advanced Materials and Composites, Colorado Springs, CO (Aug. 1986) 25-39.

2. W. L. Morris, R. V. Inman and B. N. Cox, "Microscopic Deformation in a Heated Unidirectional Graphite/Epoxy Composite," J. Materials Science, 24 (1989) 199-204.

3. D. R. Williams, D. L. Davidson and J. Lankford, "Fatigue Cracks tip Plastic Strains by the Stereoimaging Technique," Experimental Mechanics, 20 (1980) 134-139.

4. W. L. Morris, R. V. Inman and M. R. James, "Measurement of Fatigue-Induced Plasticity," J. Materials. Science, 17 (1982) 1413-1419.

5. M. R. James, W. L. Morris and B. N. Cox, "High Accuracy Automated Strain Field Mapper," Experimental Mechanics, 30 (1990) 60-67.

6. M. R. James, W. L. Morris, B. N. Cox and M. S. Dadkhah, "Description and Application of Displacement Measurements Based on Digital Image Processing," AMD-102, Micromechanics: Experimental Techniques, ed. W. N. Sharpe, Jr., ASME (1989) 89-99.

7. H. C. Tsai, A. M. Arocho and L. W. Gause, "Prediction of Fiber Matrix Interphase Properties and Their Influence on Interphase Stress, Displacement and Fracture Toughness of Composite Materials," Materials Science and Engng., A126 (1990) 295-304.